Numerical Solution of the Boundary-Layer Equations for a General Aviation Fuselage

Yong-Sun Wie*
High Technology Corporation, Hampton, Virginia 23666
and
Julius E. Harris†
NASA Langley Research Center, Hampton, Virginia 23665

Numerical solutions of the three-dimensional, compressible laminar boundary-layer equations for a general aviation fuselage are presented. The numerical procedure is second-order accurate and independent of the crossflow velocity direction. Results are presented for a Mach number and unit Reynolds number of 0.3 and 7 $\times 10^6$ m^{-1}, respectively, for angles of attack of 0 and 3 deg. Comparisons are made between results obtained using a nonorthogonal body-oriented coordinate system and a streamline coordinate system. Axisymmetric analog results are also compared with the three-dimensional solutions.

Nomenclature

C_{fx}, C_{fy} = skin friction coefficient in the x and y directions, respectively, Eq. (11)
h_1, h_2 = metric coefficients in the x and y coordinates, respectively
M_∞ = freestream Mach number
Pr = Prandtl number
p = pressure
T = temperature
u, v, w = velocity components in the x, y, and z directions, respectively
V = total velocity, Eq. (7)
X = axial distance (m) measured from the nose, see Fig. 1a
x, y, z = body-oriented coordinates (Fig. 1a) or streamline coordinates (Fig. 1b)
α = angle of attack
$\Delta x, \Delta y, \Delta \zeta$ = grid spacing in the x, y, and ζ directions, respectively
δ = boundary-layer thickness, $(z)_{V/Ve=0.995}$
δ^* = displacement thickness, defined in Eq. (13)
ζ = transformed normal coordinate
θ = angle between x and y coordinates
μ = molecular viscosity
ρ = density
ϕ = azimuthal angle, 0 and π on the windward and leeward plane of symmetry, respectively; see Fig. 1a

Subscripts

b = body-oriented coordinates
e = edge of the boundary layer
s = streamline coordinates
w = wall
y = partial differentiation with respect to y
∞ = freestream

Presented as Paper 90-0305 at the AIAA 28th Aerospace Sciences Meeting, Reno, NV, Jan. 8–11, 1990; received April 19, 1990; revision received Nov. 20, 1990; accepted for publication Dec. 12, 1990.

*Research Scientist. Member AIAA.
†Senior Research Scientist, Theoretical Flow Physics Branch, Fluid Mechanics Division. Associate Fellow AIAA.

Introduction

THREE-DIMENSIONAL boundary-layer flows have been numerically studied for over three decades. During this period, the capability to obtain numerical solutions has advanced from solving the similarity equations for relatively simple geometric shapes to the full nonsimilar equations for more complex aircraft configurations. The earliest numerical work that can be referenced, to the authors' knowledge, is that of Raetz[1] and Der and Raetz.[2] References 1 and 2 are important early contributions in that they introduced the stability of the mixed parabolic-hyperbolic system, i.e., the zone of influence dependence principle. Blottner[3] presented a state-of-the-art review of three-dimensional boundary-layer procedures that, with the exception of recently developed numerical methods, remains current at the present date. More recent treatment of the subject is presented in Refs. 4 and 5.

Over the past decade, the major emphasis in computational fluid mechanics has focused on solving the Euler and Navier-Stokes equations for increasingly more complex aerodynamic shapes. In many instances, the Navier-Stokes approach is the only viable procedure, e.g., flows with strong interaction and separation. However, Navier-Stokes solutions are generally much more expensive in terms of computer resources than boundary-layer procedures, and, while capable of simulating the physics of complex flows, are often of low resolution due to grid point restrictions and are not essential for many design and analysis procedures. The present paper addresses a finite difference procedure, independent of crossflow velocity direction, that can be efficiently applied to fuselage configurations, i.e., bodies with a symmetry plane. It should be noted that the procedure is applicable to any general configuration and has been applied to wing flows (see Ref. 6).

Results obtained from numerically solving the three-dimensional, compressible boundary-layer equations for a general aviation fuselage are presented in the present paper. Comparisons are made between numerical results obtained on a nonorthogonal body coordinate system, a streamline coordinate system, and the axisymmetric analog[7] applied to the streamline coordinate system.

Coordinate System

A nonorthogonal curvilinear system defined on the body surface is the most general boundary-layer coordinate system. The software used to generate the results presented in the present paper allows use of either the most general nonorthogonal system or any subset of the general system (see Ref. 5). In the present paper, two coordinate systems are studied: 1) a

nonorthogonal body-oriented coordinate system with crossflow planes perpendicular to the fuselage axis; and 2) an orthogonal streamline coordinate system. Schematics of the two coordinate systems are presented in Fig. 1.

Each of the selected coordinate systems has its particular advantages and disadvantages. The nonorthogonal body-oriented system is optimum from the viewpoints of grid generation and grid-spacing control. Also, in certain aspects the interface software is simpler to apply since most inviscid solutions for bodies having a plane of symmetry use one coordinate plane perpendicular to the body axis. However, the boundary-layer equations are singular at the nose of the body ($X = 0$) for the body-oriented coordinates and either special transformations such as used in Ref. 8 or other procedures must be used to isolate this singular point. The streamline coordinate system is orthogonal with zero values of crossflow velocity at the wall and edge boundaries. The system's origin is located at the stagnation point and is free of geometric singularity at the nose. The system is not independent of angle of attack and the downstream grid line distribution and grid-point spacing is difficult, if not impossible, to control without adaptive grid procedures such as that used in Ref. 9. In the present study, no attempt was made to remove the nose singularity (at $X = 0$). The singularity is isolated by locating the initial data plane slightly downstream from the nose point (see Fig. 2); consequently, the starting procedure limits the approach to small angle of attack for the blunted nose fuselage (general and commercial aircraft fuselages). For large angle of attack, transformations similar to that used in Ref. 8 can be incorporated into the initial solution procedure when using the body coordinate system.

Governing Equations

The three-dimensional, compressible boundary-layer equations for nonorthogonal curvilinear coordinates in dimensional form are as follows[5,10]:

Continuity equation:

$$\frac{\partial}{\partial x}(\rho u h_2 \sin\theta) + \frac{\partial}{\partial y}(\rho v h_1 \sin\theta) + \frac{\partial}{\partial z}(\rho w h_1 h_2 \sin\theta) = 0 \quad (1)$$

x-momentum equation:

$$\frac{\rho u}{h_1}\frac{\partial u}{\partial x} + \frac{\rho v}{h_2}\frac{\partial u}{\partial y} + \rho w \frac{\partial u}{\partial z} - \rho u^2 K_1 \cot\theta + \rho v^2 K_2 \csc\theta + \rho u v K_{12} = -\frac{\csc^2\theta}{h_1}\frac{\partial p}{\partial x} + \frac{\cot\theta \csc\theta}{h_2}\frac{\partial p}{\partial y} + \frac{\partial}{\partial z}\left(\mu \frac{\partial u}{\partial z}\right) \quad (2)$$

y-momentum equation:

$$\frac{\rho u}{h_1}\frac{\partial v}{\partial x} + \frac{\rho v}{h_2}\frac{\partial v}{\partial y} + \rho w \frac{\partial v}{\partial z} - \rho v^2 K_2 \cot\theta + \rho u^2 K_1 \csc\theta + \rho u v K_{21} = \frac{\cot\theta \csc\theta}{h_1}\frac{\partial p}{\partial x} - \frac{\csc^2\theta}{h_2}\frac{\partial p}{\partial y} + \frac{\partial}{\partial z}\left(\mu \frac{\partial v}{\partial z}\right) \quad (3)$$

Energy equation:

$$\frac{\rho u}{h_1}\frac{\partial H}{\partial x} + \frac{\rho v}{h_2}\frac{\partial H}{\partial y} + \rho w \frac{\partial H}{\partial z} = \frac{\partial}{\partial z}\left[\frac{\mu}{Pr}\frac{\partial H}{\partial z} + \mu\left(1 - \frac{1}{Pr}\right)\frac{\partial}{\partial z}\left(\frac{V^2}{2}\right)\right] \quad (4)$$

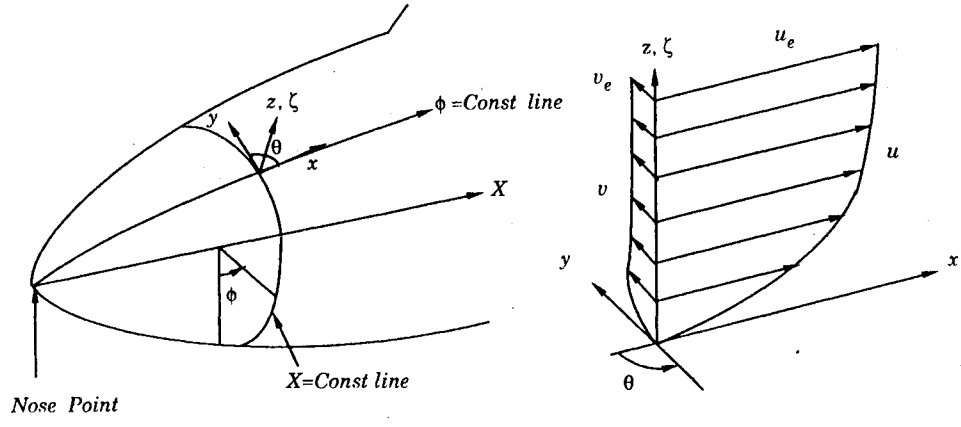

Fig. 1a Body-oriented coordinate system.

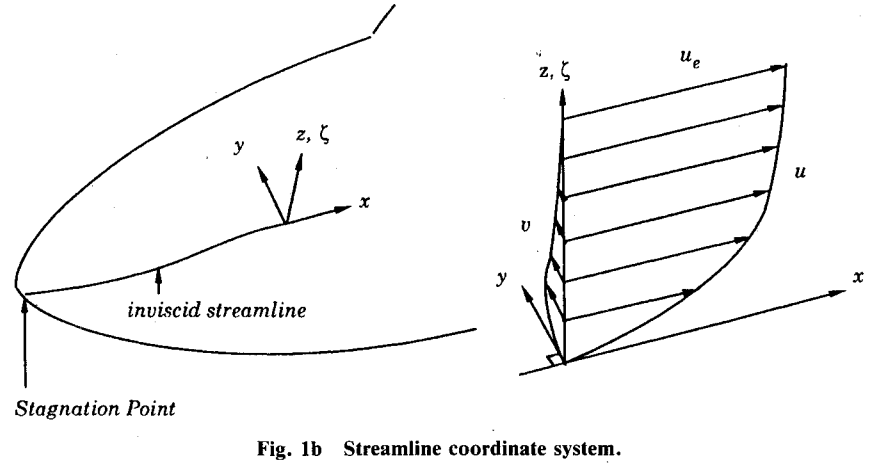

Fig. 1b Streamline coordinate system.

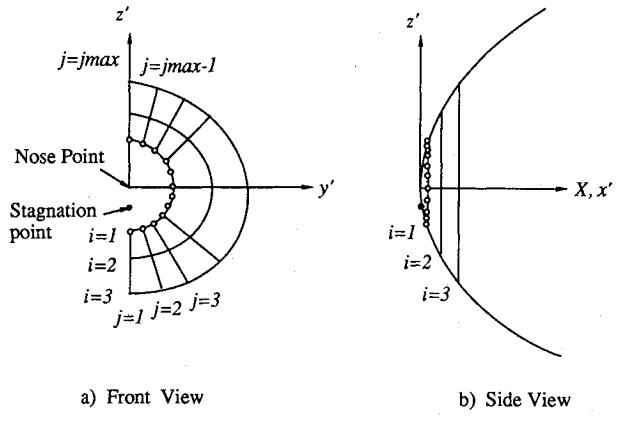

a) Front View b) Side View

Fig. 2 Initial data plane.

Here, h_1 and h_2 are metric coefficients and are functions of x and y. The parameters K_1 and K_2 are geodesic curvatures of the curves y = const and x = const, respectively, where

$$K_1 = \frac{1}{h_1 h_2 \sin\theta}\left[\frac{\partial}{\partial x}(h_2\cos\theta) - \frac{\partial h_1}{\partial y}\right] \tag{5a}$$

$$K_2 = \frac{1}{h_1 h_2 \sin\theta}\left[\frac{\partial}{\partial y}(h_1\cos\theta) - \frac{\partial h_2}{\partial x}\right] \tag{5b}$$

$$K_{12} = \frac{1}{h_1 h_2 \sin^2\theta}\left[(1+\cos^2\theta)\frac{\partial h_1}{\partial y} - 2\cos\theta\frac{\partial h_2}{\partial x}\right] \tag{6a}$$

$$K_{21} = \frac{1}{h_1 h_2 \sin^2\theta}\left[(1+\cos^2\theta)\frac{\partial h_2}{\partial x} - 2\cos\theta\frac{\partial h_1}{\partial y}\right] \tag{6b}$$

$$V = (u^2 + v^2 + 2uv\cos\theta)^{1/2} \tag{7}$$

The boundary conditions are

$$z = \delta, \quad u = u_e(x,y), \quad v = v_e(x,y), \quad H = H_e \tag{8a}$$

$$z = 0, \quad u = v = 0, \quad w = w_w$$

$$H = H_w \text{ or } \left(\frac{\partial H}{\partial z}\right)_w = 0 \tag{8b}$$

At the edge of the boundary layer, the pressure gradients are related to the inviscid velocities by the following equations:

$$\rho_e\left(\frac{u_e}{h_1}\frac{\partial u_e}{\partial x} + \frac{v_e}{h_2}\frac{\partial u_e}{\partial y} - u_e^2 K_1\cot\theta + v_e^2 K_2\csc\theta + u_e v_e K_{12}\right)$$

$$= -\frac{\csc\theta}{h_1}\frac{\partial p}{\partial x} + \frac{\cot\theta\csc\theta}{h_2}\frac{\partial p}{\partial y} \tag{9a}$$

$$\rho_e\left(\frac{u_e}{h_1}\frac{\partial v_e}{\partial x} + \frac{v_e}{h_2}\frac{\partial v_e}{\partial z} - v_e^2 K_2\cot\theta + u_e^2 K_1\csc\theta + u_e v_e K_{21}\right)$$

$$= \frac{\cot\theta\csc\theta}{h_1}\frac{\partial p}{\partial x} - \frac{\csc^2\theta}{h_2}\frac{\partial p}{\partial y} \tag{9b}$$

The perfect gas equation of state and Sutherland's viscosity are used to close the equation set. The value of the Prandtl number used in the computation is 0.72. The stagnation point and plane of symmetry equations are subsets of the governing equations and are presented in Ref. 11. The governing equations for the streamline coordinates can be obtained by equating $\theta = \pi/2$ from the equations above.

The transformation, transformed governing equations, and boundary conditions are presented in detail in Ref. 11. As previously noted, the two coordinate systems studied are subsets of the general nonorthogonal curvilinear coordinate system; consequently, the transformation is valid for both coordinate systems (body-oriented and streamline).

Numerical Method

The governing equations are solved in the transformed plane (x,y,ζ). The transformed stagnation point equations are linearized using the Newton-Raphson technique presented in Ref. 4 and discretized by a central finite difference scheme. The resulting momentum equations form a block tridiagonal system, and the energy equation becomes a tridiagonal system. The momentum equations and the energy equations are solved iteratively in a decoupled fashion. The former are solved using the Davis modified tridiagonal algorithm presented in Ref. 4. A converged solution can usually be obtained within five iterations.

The stagnation point solution is next transferred to the initial data plane: $i = 1$; $j = 1,2\ldots,j\max$ (see Fig. 2). The transfer procedure assumes that the velocity gradients at the stagnation point remain constant between the stagnation point and the initial data plane; consequently, the initial data plane must be located near the stagnation point. This restriction limits the present procedure to small angles of attack when using the body-oriented coordinate system. The transfer procedure is discussed in detail in Ref. 11.

Matsuno's finite difference method[12] is used to march away from the initial data plane. This finite difference method is an extension of the predictor-corrector form of the Crank-Nicolson scheme originally suggested by Douglas and Jones.[13] The scheme is noniterative, explicit in y, half implicit in ζ, $\mathcal{O}(\Delta\zeta^2)$ for constant $\Delta\zeta$, highly vectorizable, and independent of the sign (direction) of the crossflow velocity component. The unique characteristic of this method is that the crosswise (y) derivatives are formed independent of the sign of the crossflow velocity component. The crosswise derivatives are approximated by three-point central differencing at the previous step. This difference form yields stability independent of the crossflow direction.

Both the finite difference equations (predictor and corrector steps) for the momentum equations are cast in a 2×2 block tridiagonal form and solved by the Davis modified tridiagonal algorithm (see Ref. 4). Each (predictor and corrector) finite difference energy equation can be arranged into a linear tridiagonal matrix equation form and solved by the Thomas algorithm. Although there is coupling between the momentum and energy equations, they can be solved in an uncoupled manner due to the quasilinearization involved in the predictor and corrector scheme.

The zone of dependence principle requires

$$\frac{u}{u_e} > 0 \text{ and } \left|\frac{h_1(\Delta x)v}{h_2(\Delta y)u}\right| < 1.0 \tag{10}$$

Matsuno's finite difference scheme is conditionally stable with the same constraint as that required by the zone of dependence principle. The accuracy of this scheme is investigated in Ref. 11.

Geometry, Inviscid Solution, and Boundary-Layer Edge Condition

The semianalytic geometry program developed by Barger and Adams[14] was used for the fuselage geometry. The Hess[15] potential flow code was used to obtain the inviscid flow. The inviscid solution from the Hess code is sensitive to geometry input and exhibits oscillating behavior if the geometry is not smooth. The semianalytic geometry program used in the present investigation gives an accurate and smooth modeling for fuselage shapes.

Typical inviscid grids are shown in Fig. 3. For the present study, inviscid solutions were obtained using 54 grids in the X direction and 37 grids in the ϕ direction. The output from the

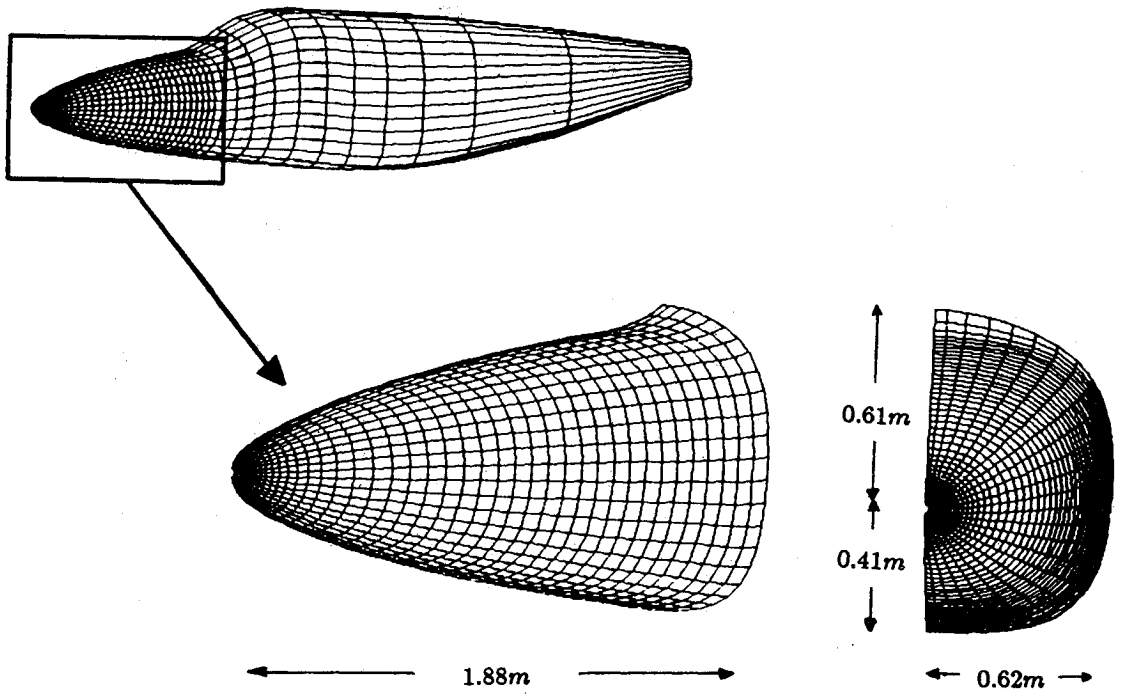

Fig. 3 Typical inviscid grids on the Cessna fuselage.

Hess code is on the centroids of the panels; consequently, the inviscid solution along the lines of symmetry must be obtained by extrapolation. A major problem encountered with the inviscid solution is that the method is not accurate in the nose region due to the singularity as $r \to 0$. Therefore, the boundary-layer calculations must be started slightly downstream from the nose point when the inviscid flowfield is obtained using panel methods.

Body-Oriented Coordinates

Using the geometry program and the inviscid solution from the Hess code, the inviscid velocity components (u_e, v_e) and the angle θ are calculated on the panel centroids. The inviscid solutions on the lines of symmetry are extrapolated from the interior region using the symmetry condition (in case of u_e). A bidirectional cubic spline with tension interpolation program is used to obtain the inviscid velocity components and the angle θ on the boundary-layer grids. Using this interpolation program, no discontinuity of the streamwise derivatives or spanwise derivatives of the inviscid velocity components was found. The metric coefficients are then obtained numerically by central differences.

Streamline Coordinates

Using the geometry program and the inviscid velocities from the Hess code, inviscid velocity components in the spherical polar coordinate system are calculated. Next, the streamline coordinates are calculated using the method developed by Hamilton et al.[16] The metric coefficient h_2 is calculated numerically by central differences. Using the same extrapolation and interpolation procedures as used for the body-oriented coordinates, the inviscid velocity (u_e) is obtained on the streamline grids. The streamlines originate slightly downstream from the stagnation point. It is to be noted that the origin for each streamline must be on the same x; i.e., the initial x direction and y direction must be orthogonal to each other.

Results and Discussion

The fuselage forebody selected for the present investigation is nonanalytic and contains nonsmooth areas typical of many general aviation aircraft fuselage shapes. The case is particularly interesting in that the crossflow is into the plane of symmetry: $v_e < 0$ as $\phi \to 0$; $v_e > 0$ as $\phi \to \pi$. Consequently, standard marching procedures, such as traditionally used on cones, ellipsoid of revolution, etc., at angle of attack cannot be easily used to advance the solution into the crossflow plane; i.e., $x = \text{const}$, $y = y_2, y_3, \ldots, y_{j\max-1}$.

Test Conditions

Numerical results are presented for a Mach number and unit Reynolds number of 0.3 and 7×10^6 m^{-1}, respectively, for 0- and 3-deg angles of attack for an adiabatic wall. A schematic of a typical panel distribution used to obtain the inviscid solution is presented in Fig. 3. Boundary-layer grids for the body-oriented coordinate system using 31 grids in the y direction and the streamline coordinate system using 91 streamlines are shown in Figs. 4 and 5, respectively. The 91 grid-point distribution (in the y direction) for the streamline coordinate system presented in Fig. 5 is used for the results presented in the present paper for the good resolution on the side of the fuselage.

The skin friction coefficients are defined as

$$C_{fx} = \frac{(\mu \partial u/\partial z)_w}{\frac{1}{2}\rho_e V_e^2}, \quad C_{fy} = \frac{(\mu \partial v/\partial z)_w}{\frac{1}{2}\rho_e V_e^2} \tag{11}$$

The skin friction coefficients presented in the present paper are referenced to the body-oriented coordinate system. Results obtained in the streamline coordinate system have been transformed to the body-oriented coordinate system as follows:

$$(C_{fx})_b = (C_{fx}^2 + C_{fy}^2)_s^{1/2} [\cos(\beta + \gamma) - \sin(\beta + \gamma) \cot\theta]$$
$$(C_{fy})_b = (C_{fx}^2 + C_{fy}^2)_s^{1/2} \sin(\beta + \gamma) \csc\theta \tag{12}$$

where $\beta = \tan^{-1}(C_{fy}/C_{fx})_s$ and γ is an angle between the streamline coordinate line ($y = \text{const}$) and the body-oriented coordinate line ($y = \text{const}$). Displacement thickness, as presented in the present paper, was obtained from the following definition:

$$\delta^* = \int_0^{z_e} \left(1 - \frac{\rho V}{\rho_e V_e}\right) dz \tag{13}$$

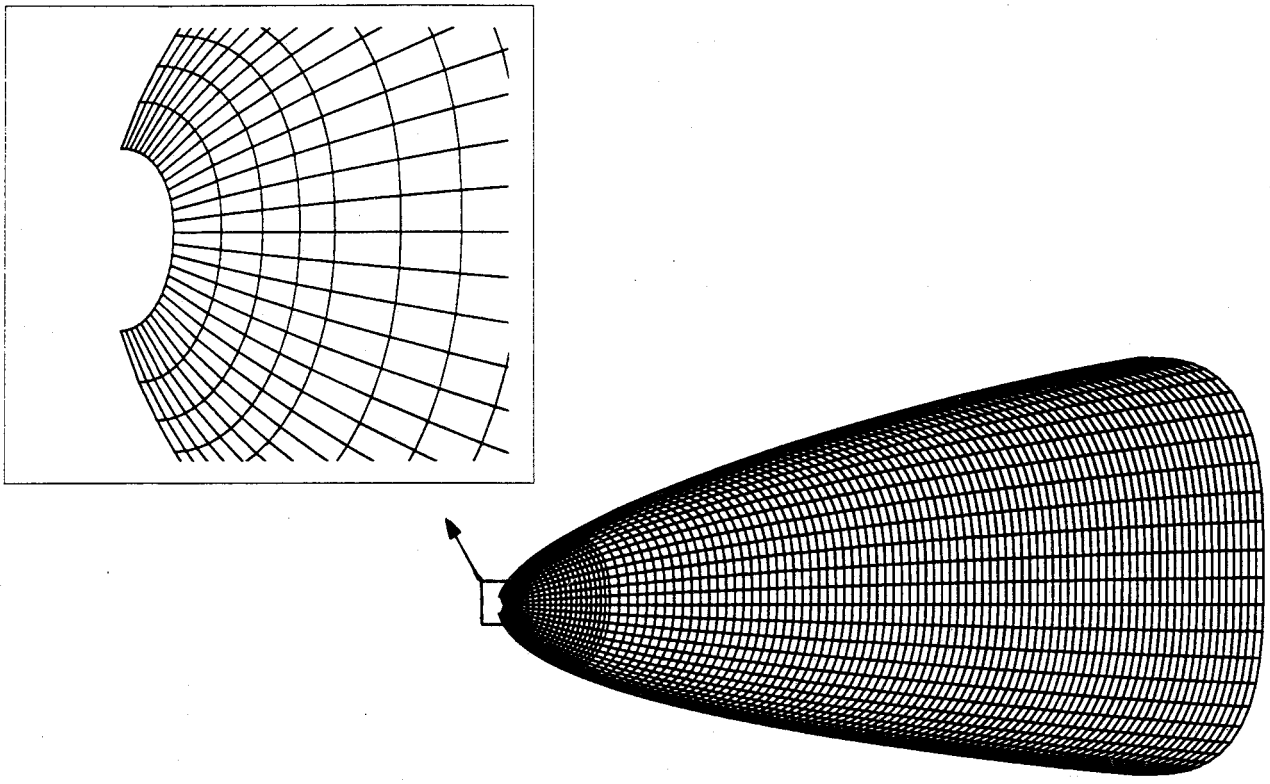

Fig. 4 Body-oriented boundary-layer grids.

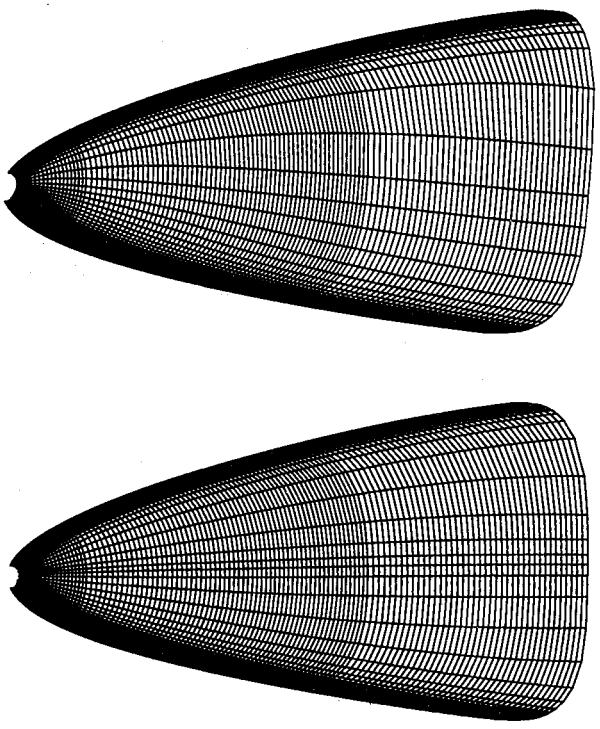

Fig. 5 Streamline boundary-layer grids: a) $\alpha = 0$ deg, b) $\alpha = 3$ deg.

Boundary-Layer Grid

A uniform $\Delta\zeta$ distribution having a value of 0.2 was used in the present study. The software automatically adds additional grid points in the direction normal to the wall, if required, as solution proceeds downstream. For the present calculations, ζ_e varied from 3.0 near the stagnation point to 6.0 at $X = 1.5$. The stepsize in x varied from 0.001 near the stagnation point to 0.03 downstream, requiring about 110 steps. The grid distribution in y was dependent on the coordinate system. Numerical experimentation was required to determine the grid distribution that assured that the solution was grid independent. It was found that 31 uniformly distributed points in the y direction produce grid independent results for the nonorthogonal body coordinate system. Similar studies of the streamline coordinate system showed that 91 uniformly distributed points near the stagnation point were required to produce grid independent results. The factor of three increase in the number of points in the y direction for the streamline coordinate system as compared with the body-oriented system is due to the lack of control of the grid spacing downstream. This problem can be solved using adaptive grid control procedures, but the adaptive approach adds complexity to the software without providing any advantage as compared with the nonorthogonal body-oriented system.

The net CPU time for solving the governing equation for a grid of $110 \times 31 \times 31$ points on the CRAY-2 was 8 s. The time and cost associated with solving the three-dimensional boundary-layer equations is small as compared with that required modeling the geometry and obtaining the inviscid flowfield.

The softwares used in the present study were developed by the authors in support of transition prediction software. The general curvilinear coordinate system was selected in order to provide users of the software with the widest possible choice of coordinate systems. In the present study, the nonorthogonal body coordinate system was selected because of the following factors: 1) angle of attack independence, 2) ease of using geometry data specified for fuselage shapes, and 3) ease of using most inviscid software. The streamline coordinate system is angle-of-attack dependent and was chosen for study since several of the transition prediction procedures required output from the viscous solution along the streamline trajectories. For typical wing flows, the direction of the group velocity for spatial stability analysis can be approximated as that of the streamlines (see Ref. 17). Consequently, interpolation errors could be minimized in obtaining the viscous data, required for stability analysis, from the data base generated by the boundary-layer solution. However, this approximation cannot be made for fuselage shapes. Therefore, interpolation of the

viscous flowfield data base in both x and y is required for both coordinate systems. Experience gained in the present study indicates that there is no advantage in using the streamline coordinate system for general aircraft fuselage shapes.

A comment that must be made concerns the axisymmetric analog results presented in Ref. 18. The axisymmetric analog results and comments based on these results in Ref. 18 are not correct. The axisymmetric analog results presented in Ref. 18 were inadvertently obtained from the 31 streamline data base instead of the grid-independent 91 streamline results. The axisymmetric results presented in the present paper were generated from the data base using 91 streamlines. The metric coefficient h_2 is obtained using central differences and cannot be accurately calculated for 31 streamlines on the side of fuselage.

Zero-Deg Angle of Attack

A side view of the fuselage forebody is presented in Fig. 6 showing the maximum pressure line and the crossflow velocity (based on the body-oriented coordinate system) regions. The lines of symmetry, $\phi = 0$ and π, are inflow lines; consequently, standard marching procedures cannot be easily used to advance the solution from the lines of symmetry into the interior region (x = const; $y = y_2, y_3, \ldots, y_{j\max-1}$). However, as previously discussed, the present method is independent of the sign of the crossflow velocity.

Numerical results are presented in Figs. 7-9 for $\alpha = 0$ deg. The agreement between the skin friction coefficients obtained in the two coordinate systems is excellent over the entire surface. The axisymmetric analog results agree with the three-dimensional results (body-oriented coordinate and streamline coordinate systems) to within 10% and have the correct trend on the side of the fuselage.

Boundary-layer thickness (Fig. 8) and displacement thickness (Fig. 9) results exhibit similar trends in agreement between the results obtained in the two coordinate systems and the axisymmetric analog.

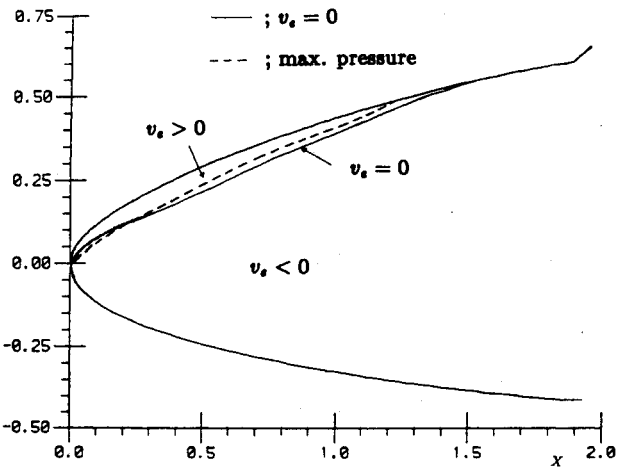

Fig. 6 Sign of inviscid crossflow velocity component ($M_\infty = 0.3$, $\alpha = 0$ deg).

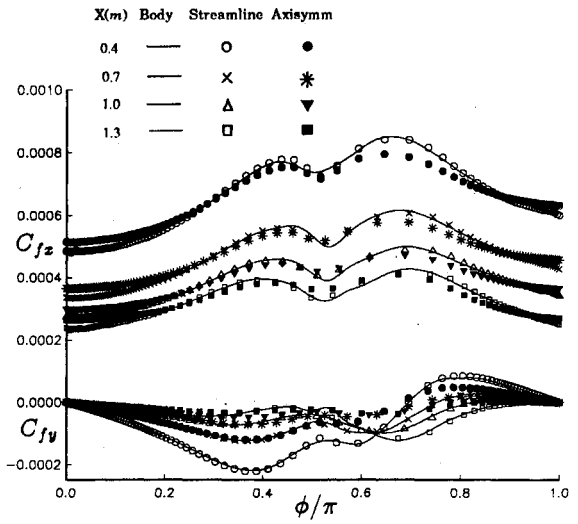

Fig. 7 Skin friction coefficient ($M_\infty = 0.3$, $\alpha = 0$ deg).

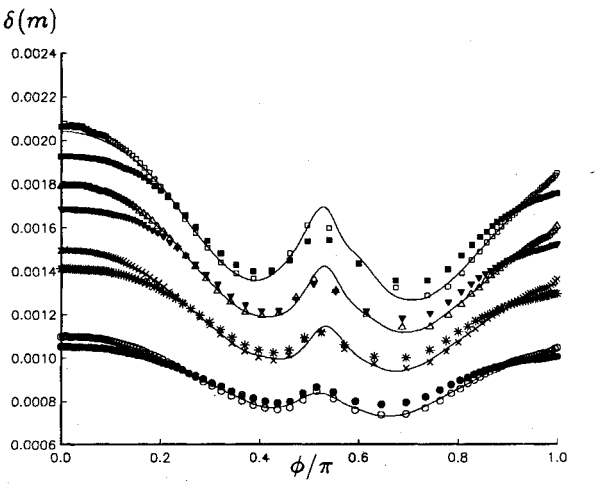

Fig. 8 Boundary-layer thickness ($M_\infty = 0.3$, $\alpha = 0$ deg).

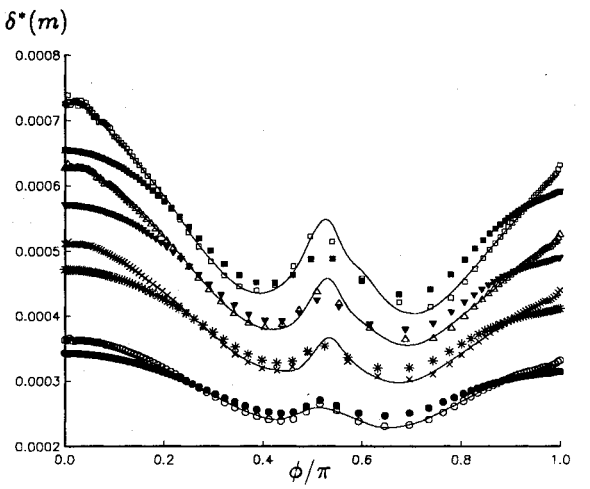

Fig. 9 Displacement thickness ($M_\infty = 0.3$, $\alpha = 0$ deg).

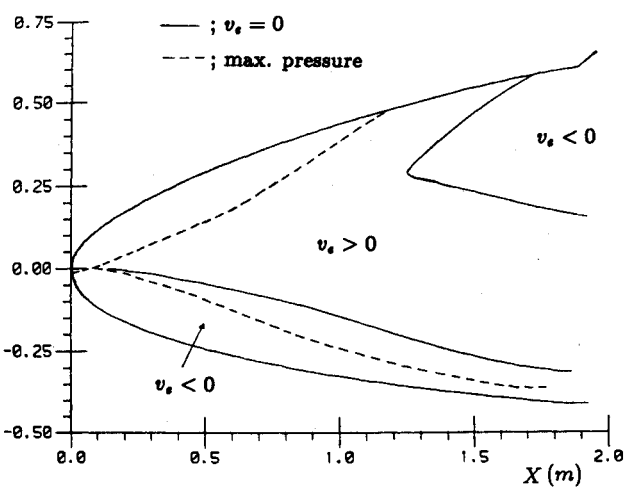

Fig. 10 Sign of inviscid crossflow velocity component ($M_\infty = 0.3$, $\alpha = 3$ deg).

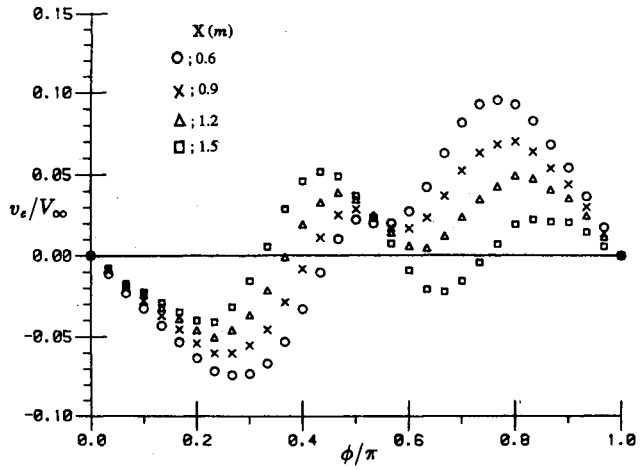

Fig. 11 Inviscid crossflow velocity component (v_e) as a function of ϕ ($M_\infty = 0.3$, $\alpha = 3$ deg).

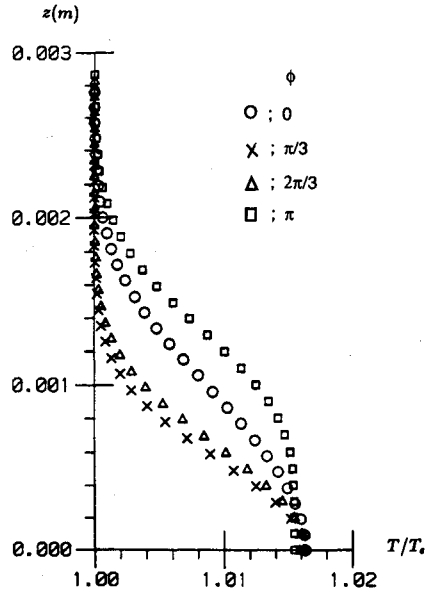

Fig. 14 Temperature profile at $X = 1.5$ ($M_\infty = 0.3$, $\alpha = 3$ deg).

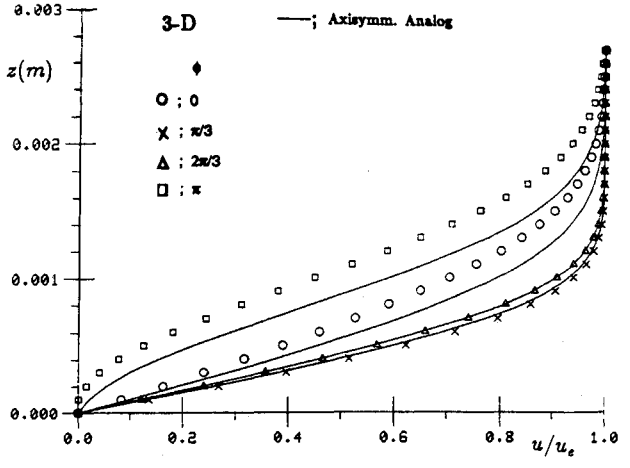

Fig. 12 Streamwise velocity profile at $X = 1.5$ ($M_\infty = 0.3$, $\alpha = 3$ deg).

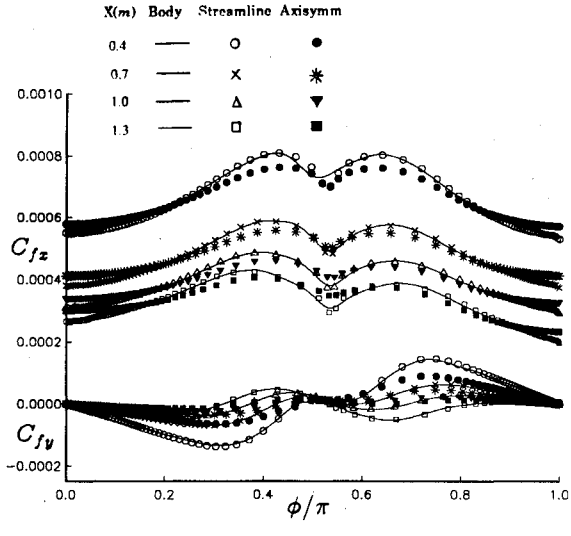

Fig. 15 Skin friction coefficients ($M_\infty = 0.3$, $\alpha = 3$ deg).

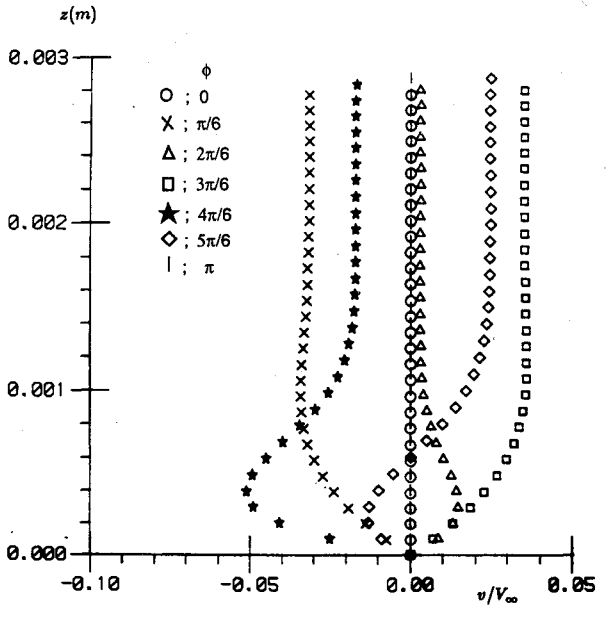

Fig. 13 Crossflow velocity profile at $X = 1.5$ ($M_\infty = 0.3$, $\alpha = 3$ deg).

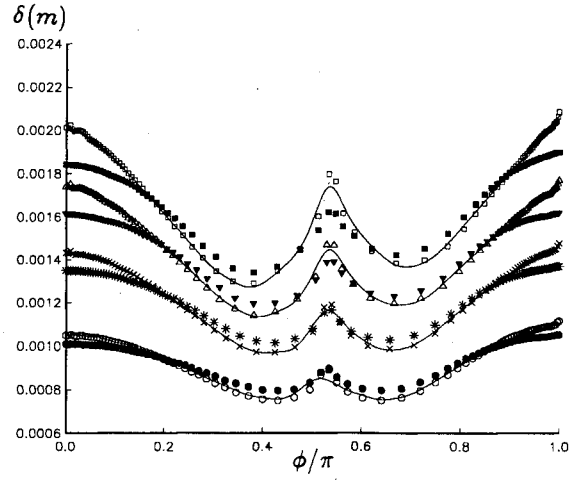

Fig. 16 Boundary-layer thickness ($M_\infty = 0.3$, $\alpha = 3$ deg).

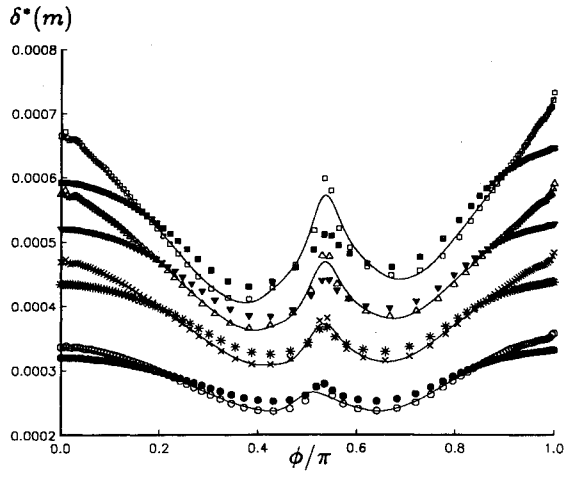

Fig. 17 Displacement thickness ($M_\infty = 0.3$, $\alpha = 3$ deg).

Three-Deg Angle of Attack

At this angle of attack, the flowfield has two relative maxima pressure lines for $0 \leq \phi \leq \pi$ with multiple changes in the sign of the crossflow velocity (v_e) based on the body-oriented coordinates; see Fig. 10. Figure 11 shows the values of v_e/V_∞ as a function of ϕ at $X = 0.6$, 0.9, 1.2, and 1.5. The sign of v_e in the interval $0 \leq \phi \leq \pi$ changes three times at $X = 1.5$. Streamwise velocity profiles (based on the body-oriented coordinates) are presented and compared with axisymmetric analog results in Fig. 12 for $X = 1.5$. The agreement is seen to be reasonably good off the plane of symmetry with the largest disagreement occurring at the leeward plane where the flow tends to separation. Crossflow and temperature profiles are presented in Figs. 13 and 14, respectively.

Skin friction coefficients, boundary-layer thickness, and the displacement thickness results are presented in Figs. 15–17. The agreement between the numerical results in the body-oriented and the streamline coordinate systems is also excellent over the entire surface. The axisymmetric analog results are compared with the three-dimensional results in Figs. 15–17. The agreement between the axisymmetric analog results and the three-dimensional boundary-layer results is nearly of the same order as for 0-deg angle of attack.

Concluding Remarks

The three-dimensional, compressible, laminar boundary-layer equations were numerically solved for the forebody of a general aviation aircraft fuselage. Solutions were obtained for a Mach number and unit Reynolds number of 0.3 and 7×10^6 m^{-1}, respectively, for angles of attack of 0 and 3 deg. Numerical solutions were obtained using two coordinate systems: 1) nonorthogonal body-oriented and 2) streamline. Axisymmetric analog results were also obtained from the streamline system.

The crossflow velocity direction for the fuselage was into the plane of symmetry for both the most windward and leeward planes for both angles of attack considered. Consequently, standard solution procedures that march around the body using the plane of symmetry as an initial data plane could not be easily used to solve the present test case. However, no numerical problems were encountered using the finite difference procedure used in the present analysis. It should also be noted that at 3-deg angle of attack the crossflow velocity component reversed direction as often as three times in the region bounded by the windward and leeward symmetry planes.

The agreement of the boundary-layer parameters obtained in the two coordinate systems was excellent over the entire surface; however, three times as many grid points were required for the streamline system to achieve grid independent results. The streamwise skin friction coefficient results obtained from the axisymmetric analog solution agreed closely in trend and magnitude with the three-dimensional results. Similar agreement was obtained for the boundary-layer thickness, displacement thickness, and streamwise velocity profiles, with maximum disagreement occurring on the plane of symmetry.

The following comments can be made in relation to the two coordinate systems: 1) the streamline system requires more computational effort than the body-oriented system; 2) the body-oriented system is independent of the angle of attack; 3) it is difficult, if not impossible, to control the streamline distribution downstream; and 4) there is no advantage in using the streamline system in relation to transition prediction procedures for fuselage shapes.

Acknowledgment

This research was supported by NASA Grant NAS1-18240.

References

[1]Raetz, G. S., "A Method of Calculating Three Dimensional Laminar Boundary-Layers of Steady Compressible Flows," Northrop Corp., Rept. NAI-58-73(BLC-114), Dec. 1957.

[2]Der, J., Jr., and Raetz, G. S., "Solution of General Three-Dimensional Laminar Boundary-Layer Problems By an Exact Numerical Method," Inst. of the Aerospace Sciences Annual Meeting, Paper 62-70, New York, Jan. 1962.

[3]Blottner, F. G., "Computational Techniques for Boundary Layers," AGARD Lecture Series, No. 73, Feb. 1975.

[4]Blottner, F. G., "Introduction to Computational Techniques for Boundary Layers," Sandia Lab., Rept. SAND-79-0893, Albuquerque, NM, 1979.

[5]Hirschel, E. H., and Kordulla, W., "Shear Flow in Surface-Oriented Coordinates," *Notes on Numerical Fluid Mechanics*, Vol. 4, F. Vieweg & Sons, Braunschwein, Germany, 1981.

[6]Woodson, S., Campbell, J., and DeJarnette, F. R., "An Interactive Three-Dimensional Boundary-Layer Method for Transonic Flow Over Swept Wings," AIAA Paper 89-0112, Jan. 1989.

[7]Cooke, J. C., "An Axially Symmetric Analogue for General Three-Dimensional Boundary-Layers," British Aeronautical Research Council, R. & M. No. 3200, London, June 1961.

[8]Cebeci, T., Khattab, A. K., and Stewartson, K., "Three-Dimensional Laminar Boundary Layers and OK of Accessibility," *Journal of Fluid Mechanics*, Vol. 107, 1981, pp. 57–87.

[9]Wie, Y. S., and DeJarnette, F. R., "Numerical Investigation of Three-Dimensional Flow Separation Using the Boundary Layer Equations," AIAA Paper 88-0617, Jan. 1988.

[10]Cebeci, T., Kaups, K., and Ramsey, J. A., "A General Method for Calculating Three-Dimensional Compressible Laminar and Turbulent Boundary Layers on Arbitrary Wings," NASA CR-2777, Jan. 1977.

[11]Wie, Y. S., "A Three-Dimensional, Compressible, Boundary-Layer Method for General Fuselages," Vol. I, Numerical Method, Vol. II, User's Manual, NASA CR-4292, May 1990.

[12]Matsuno, K., "A Vector-Oriented Finite Difference Scheme for Calculating Three-Dimensional Compressible Laminar and Turbulent Boundary Layers on Practical Wing Configurations," AIAA Paper 81-1020, June 1981.

[13]Douglas, J., Jr., and Jones, B. F., "On Predictor-Corrector Methods for Nonlinear Parabolic Differential Equations," *Journal of the Society for Industrial and Applied Mathematics*, Vol. 11, No. 1, 1963, pp. 195–204.

[14]Barger, R. L., and Adams, M. S., "Semianalytic Modeling of Aerodynamic Shapes," NASA-TP 2413, April 1985.

[15]Hess, J. L., "Calculation of Potential Flow About Arbitrary 3-D Lifting Bodies," Douglas Aircraft Co., MDC J5670-01, Long Beach, CA, Oct. 1972.

[16]Hamilton, H. H., DeJarnette, F. R., and Weilmuenster, K. J., "Application of Axisymmetric Analogue for Calculating Heating in Three-Dimensional Flows," AIAA Paper 85-0245, Jan. 1985.

[17]Mack, L. M., "On the Stability of the Boundary Layer on a Transonic Swept Wing," AIAA Paper 79-0264, 1979.

[18]Wie, Y. S., and Harris, J. E., "Numerical Solution of the Boundary-Layer Equations for a General Aviation Fuselage," AIAA Paper 90-0305, Jan. 1990.